I&EC research
Industrial & Engineering Chemistry Research

Article

pubs.acs.org/IECR

Control of the Damping Properties of Magnetorheological Elastomers by Using Polycaprolactone as a Temperature-Controlling Component

Xinglong Gong,* Yanceng Fan, Shouhu Xuan,* Yangguang Xu, and Chao Peng

CAS Key Laboratory of Mechanical Behavior and Design of Materials, Department of Modern Mechanics, University of Science and Technology of China, Hefei 230027, China

ABSTRACT: A novel kind of magnetorheological elastomers (MREs) with controllable damping properties was developed in this study. Polycaprolactone (PCL) was selected as the temperature-controllable component in the *cis*-polybutadiene rubber (BR) based MREs. Several samples with different BR/PCL mass ratio matrixes were prepared. The dynamic performances of the samples, including loss factor, shear storage modulus, and loss modulus, were measured with a rheometer. Differential scanning calorimetry (DSC) analysis indicated that PCL is a phase change material and it can transform from a semicrystalline solid to a liquated soft material by increasing the surrounding temperature above the PCL melting point. Experimental results showed that the damping properties of the MREs can be controlled by varying the PCL weight ratio, the temperature, and the magnetic field. The controlling mechanism was proposed and the influence factors were analyzed. Last, it was also observed that the magneto-induced modulus and the MR effect of the MREs were changed remarkably by the added PCL under different temperatures.

1. INTRODUCTION

Magnetorheological (MR) materials are magnetically active materials whose rheological or mechanical properties can be changed continuously, rapidly, and reversibly by applying a magnetic field.[1−14] MR elastomers (MREs) mainly contain elastomers or rubberlike materials and soft magnetic particles. As soon as the two precursors are well mixed, an external magnetic field is applied to the polymer composite during the cross-linking process, so that the particle chain (columnar) structures are formed and locked into the matrix upon final cure.[4,6,9,10] The MR elastomers exhibit good MR effects and good mechanical performances; thus they have attracted increasing attention and have obtained wide application prospects.[8,10,11,15−23]

Typical applications are MRE adaptive tuned vibration absorbers,[15−19] MR fluid (MRF)−MRE vibration isolators and dampers,[20,21] and MRE isolators.[22,23] It is noted that the performances of these MRE devices are highly dependent on the damping properties (loss factor) of the MRE materials. For the MRE based vibration isolators, when the excitation signal is in the resonance frequency band of the system, more vibration energy can be dissipated by increasing the loss factor of the MREs, which is good for suppressing the amplitude expansion. In the vibration isolation frequency band of the system, a low loss factor can lead to better vibration isolation effectiveness. Thus, to obtain a desirable vibration effect, it is significant to study the controllability of the MRE damping properties. However, during the past decade, only a few works have been reported on this point. Zhou[2] indicated that the change of the loss factor could be neglected under different applied magnetic fields. Lokander et al. studied the influence of magnetic field on the loss factors of MREs, and found that the change of the loss factor was too small to be of any practical importance.[13] Recently, we also observed that the influence of magnetic field on the loss factor is small.[24] Therefore, the development of other methods to control the damping properties of the MREs is highly desirable.

It is noted that the loss factor change of the MR gels[25] is bigger than that of the MREs[2,13,24] with increasing magnetic field. Usually, the molecular chains of the MRE matrix are highly cross-linked, and the magnetic particles are restricted in the hard matrix even under the applied magnetic field. When a gel-like polymer is used as the matrix, the magnetic particles are movable under the applied magnetic field. The rearranged magnetic particles will result in the alteration of energy dissipation of the materials. Thus, the damping properties of polymer gels can be controlled by applying a magnetic field. However, the shape of gels is variable and the stiffness is too small, which is disadvantageous in practical application. To this end, the introducing of soft material into the MRE matrix may be one of the solutions, which can not only improve the damping properties but also maintain the material strength. Polycaprolactone (PCL) is a typical thermoplastic polymer, which is a semicrystalline solid and a liquated soft material when the temperatures are below and above the melting point, respectively. Due to its low phase change temperature (about 55 °C), it has been widely applied in various areas, such as shape memory polymers,[26,27] modifying agents,[28] and reversible adhesives.[29,30] Although PCL is a kind of biodegradable material, the degradability of PCL should be carried out upon enzyme catalysis in a phosphate buffer (pH 7.4) and more than 110 weeks are needed.[31,32] PCL can maintain its shape well after thermal treatment. If the PCL materials are blended into the matrix, the damping properties of the MREs can be controlled by both the temperature and the magnetic field. PCL

Received: February 6, 2012
Revised: April 15, 2012
Accepted: April 19, 2012
Published: April 19, 2012

   dx.doi.org/10.1021/ie300317b | *Ind. Eng. Chem. Res.* 2012, 51, 6395−6403

shows a high stability; thus the durability of the PCL-blended MREs will not be reduced in an atmospheric environment. To this end, the introduction of the phase change material into the MR material endows them with many unique properties, which will further enlarge their practical applications.

In this study, PCL was employed as the damping-controlling additive in the *cis*-polybutadiene rubber (BR) based MREs. The influences of mass ratios (BR/PCL), magnetic field, and temperature on the dynamic mechanical properties were systematically analyzed. The damping of this novel MRE was studied, and a controllable mechanism was proposed. In addition, the tensile strength, the modulus, and the MR effect were also evaluated.

2. EXPERIMENTAL DETAILS

2.1. Preparation of Samples. The matrix material BR was purchased from Shanghai Gao-Qiao Petrochemical Corp., China; PCL (type 800c) with an average molecular weight of 8.0×10^4 g/mol was manufactured by Shenzhen BrightChina Industrial Co.,Ltd. The magnetic particles were carbonyl iron particles (type CN) with an average diameter of 6 μm, bought from BASF. In this study, four different mass ratio (BR/PCL) matrixes, 100:0, 95:5, 90:10, and 80:20, were used to fabricate the samples. Two groups of the samples were prepared: one group with weight fractions of 60% carbonyl iron particles, which were named as MRE samples, and the other group without carbonyl iron particles, which were named as contrast samples. For the samples with four different BR/PCL mass ratio matrixes, the MRE samples were defined as nonblended MRE, PCL-blended MRE (95−5), PCL-blended MRE (90−10), and PCL-blended MRE (80−20), respectively, and the contrast samples were also defined as nonblended contrast, PCL-blended contrast (95−5), PCL-blended contrast (90−10), and PCL-blended contrast (80−20), respectively.

The fabrication of the MREs consists of mixing, preforming configuration, and curing, three major steps. First, 100 phr matrix materials (BR and PCL) were mixed homogeneously using a two-roll mill (Taihu Rubber Machinery Inc., China, Model XK-160) at room temperature. Then, the iron particles (60 wt %) and some additives (100 phr naphthenic oil, 5 phr ZnO, 1 phr stearic acid, 2 phr diaminodiphenylmethane, 5 phr sulfur, and 1 phr *N*-cyclohexyl-2-benzothiazolesulfenamide) were put into the matrix. For the preforming configuration, the mixture was put into a mold under an external magnetic field of 1300 mT at 130 °C for 10 min. The external magnetic field was generated by a self-developed magnet−heat couple device.[33] Finally, the samples were vulcanized on a flat vulcanizer (Bolon Precision Testing Machines Co., China, Model BL-6170-B) at 160 °C for 15 min under a pressure of approximately 13 MPa. The fabrication process of the contrast samples is similar to the above process except for adding the iron particles.

2.2. Thermal Properties of Samples. The melting and crystallization processes of the samples were studied by differential scanning calorimetry (DSC Q2000). All operations were performed under a nitrogen atmosphere. The sample was heated from 0 to 120 °C at a heating rate of 10 °C/min, held for 5 min to erase the previous thermal history, and cooled to 0 °C at a cooling rate of 10 °C/min. Then, the heating and cooling processes were operated again.

2.3. Observation of Microstructure. The microstructures of the samples were observed by using an environmental scanning electron microscope (SEM; Philips of Holland, Model XL-30 ESEM). These samples were cut into flakes and coated with a thin layer of gold prior to the SEM observation. The accelerating voltage was set at 15 kV.

2.4. Testing of the Tensile Strength. The tensile strength of the samples was tested by using an electronic tensile machine (Jiangdu Jingcheng Test Instruments Factory, China, Model JPL-2500) at room temperature. Each sample was cut into a dumbbell, with a thickness of 2 mm and a middle width of 6 mm. The stretching rate was 500 mm/min.

2.5. Measurement of Dynamic Properties. The dynamic mechanical performances of these samples were measured by using a rheometer (Physica MCR 301, Anton Paar). A sample was set between the rotating disk and the base. When the rotating disk rotated, the sample was in a shear deformed mode, and there was no sliding between the rotating disk and the sample. The magnetic field strength, which was parallel with the thickness direction of the sample, was adjusted by controlling the current values supplied to the electromagnetic coil.

In the experiment, the samples had dimensions of 10 mm radius and 1 mm thickness, in which the particle chains were distributed along the thickness direction. The samples were tested under different temperatures (25, 30, 40, 50, 60, 70, 80, and 90 °C), which were controlled by a fluid circulator with water. Three testing types were used to measure the dynamic properties of the samples under different temperatures. The conditions for these types are listed as follows:

(a) Magnetic field dependence testing: The frequency was 10 Hz, the shear strain amplitude was 0.5%, and the magnetic field was swept from 0 to 1000 mT.
(b) Shear strain amplitude dependence testing: The frequency was 10 Hz, the magnetic fields were 0 mT and 500 mT, respectively, and the shear strain amplitude was swept from 0.1 to 1.5%.
(c) Frequency dependence testing: The shear strain amplitude was 0.5%, fields were 0 mT and 500 mT, respectively, and the frequency was swept from 1 to 20 Hz.

3. RESULTS AND DISCUSSION

The carbonyl iron particles were mixed into the rubber matrix, and they were well dispersed in the rubber homogenously. Then, the composite was preconfigurated and the iron particles could form chainlike structures within the rubber matrix under application of a magnetic field. After vulcanization, the MRE sample with allied magnetic particle chains (Figure 1) was

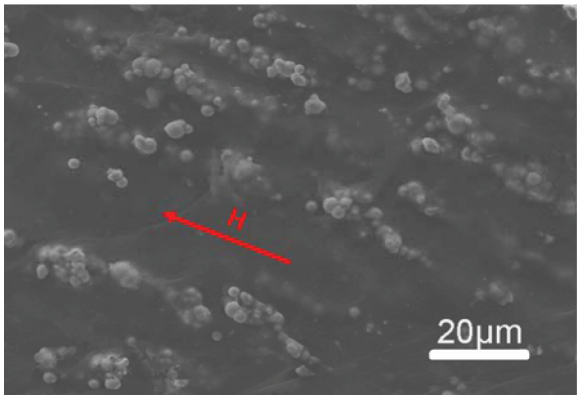

Figure 1. Micrograph of the MRE sample. The red arrow represents the direction of the particle chains which is parallel with the applied magnetic field.

dx.doi.org/10.1021/ie300317b | *Ind. Eng. Chem. Res.* 2012, 51, 6395−6403

prepared. For most of the previously reported MREs, the change of loss factor was small. To enlarge the controllability, PCL was employed as the temperature-controllable component to vary the damping properties of the MREs. Here, several samples with different BR/PCL mass ratio matrixes were prepared, their microstructures were observed, and the dynamic properties were also characterized.

3.1. Microstructure and Tensile Strength. SEM micrographs of the samples are shown in Figure 2, where parts a and b correspond to the nonblended contrast and the nonblended MRE, respectively, parts c and e correspond to the PCL-blended contrast (80−20), and parts d and f correspond to the PCL-blended MRE (80−20). From Figure 2b,d,f, the particle chains in the matrix can be observed. Figure 2a,b shows the micrographs of the nonblended samples, and the smooth cross section can be seen. When the PCL is added into the BR matrix, the PCL shows the long threadlike structures in the matrix, and the pit and protrusion in the cross section of the PCL-blended samples can be clearly observed (Figure 2c−f).

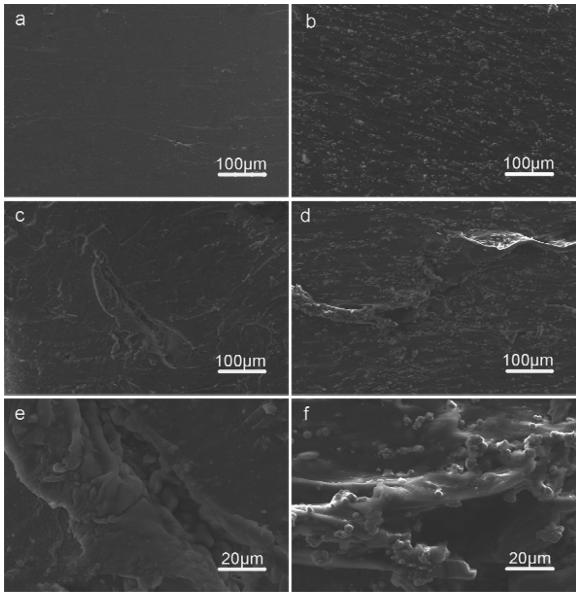

Figure 2. SEM images of the samples: (a) nonblended contrast; (b) nonblended MRE; (c, e) PCL-blended contrast (80−20); (d, f) PCL-blended MRE (80−20).

The influence of temperature on the characteristic of the PCL matrix was studied. Figure 3 shows the phase change of the PCL by using differential scanning calorimetry (DSC). DSC curves of pure PCL and of the nonblended contrast, PCL-blended contrast (80−20), and PCL-blended MRE (80−20) are given in Figure 3. During the cooling process, all the other samples except for the nonblended contrast have an exothermic peak located around 26 °C, which is the crystallization point of PCL. Thus, PCL is in a semicrystalline solid state at room temperature. Furthermore, in comparison to the nonblended contrast, the other samples have an endothermic peak during the heating process. This indicates that the PCL in pure PCL, PCL-blended contrast (80−20), and PCL-blended MRE (80−20) has melted and the melting points are 56.59, 54.43, and 52.75 °C, respectively. For the PCL-blended MRE, the melting point of PCL is low and can be carried out easily in practical application. Slight shifts of the endothermic and exothermic peaks are found, which indicates that BR/PCL blend systems

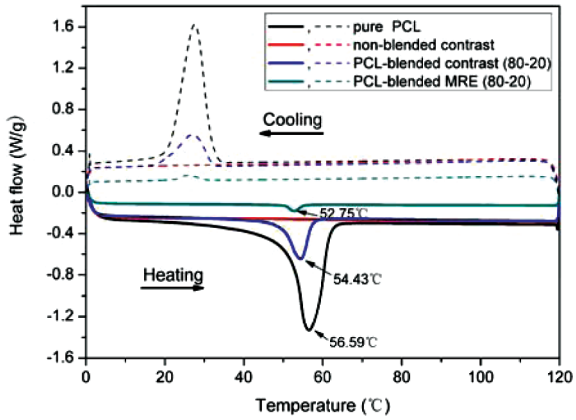

Figure 3. DSC curves of pure PCL as well as the nonblended contrast, PCL-blended contrast (80−20), and PCL-blended MRE (80−20).

are immiscible.[34,35] The compatibility between PCL and BR is poor when PCL is in a semicrystalline solid state; thus PCL can be pulled out from the BR matrix. As a result, the pit and protrusion can be formed in the cross section of sample (Figure 2c−f).

The effect of PCL content on the tensile strength of the MRE samples was also studied (Figure 4). With increasing PCL, the tensile strength decreases and then increases. For the poor compatibility between BR and PCL, the tensile strength decreases when PCL is added. However, network structures of PCL in the BR matrix might be formed when the PCL content increases gradually. Thus, the tensile strength shows an increased tendency when the PCL content is above 5 phr.

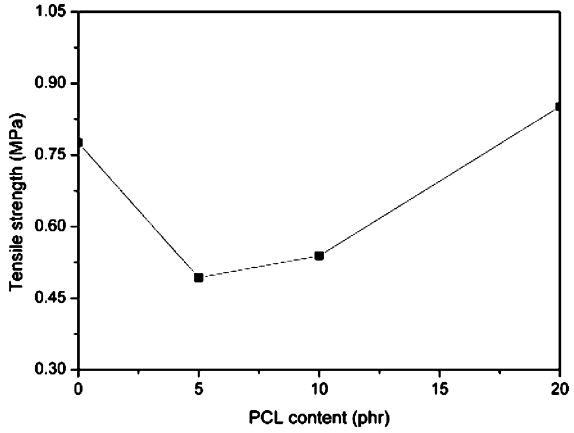

Figure 4. Tensile strength of MRE samples with different PCL contents.

3.2. Loss Factor. *3.2.1. Loss Factor under Different Temperatures and Magnetic Field Strengths.* The loss factors of the samples under different temperatures are shown in Figure 5. All tests were conducted at a frequency of 10 Hz, constant shear strain amplitude of 0.5%, and constant magnetic field strength of 0 mT. It can be seen that the loss factors of the nonblended samples (nonblended contrast and nonblended MRE) decrease gradually with increasing temperature, which is the characteristic of a cross-linked polymer. When PCL is added into the BR matrix, the loss factor suddenly increases at 60 °C. The movement of PCL molecular chains sharply increases when PCL transforms from a semicrystalline solid to a liquated soft material; the energy dissipation suddenly increases

dx.doi.org/10.1021/ie300317b | Ind. Eng. Chem. Res. 2012, 51, 6395−6403

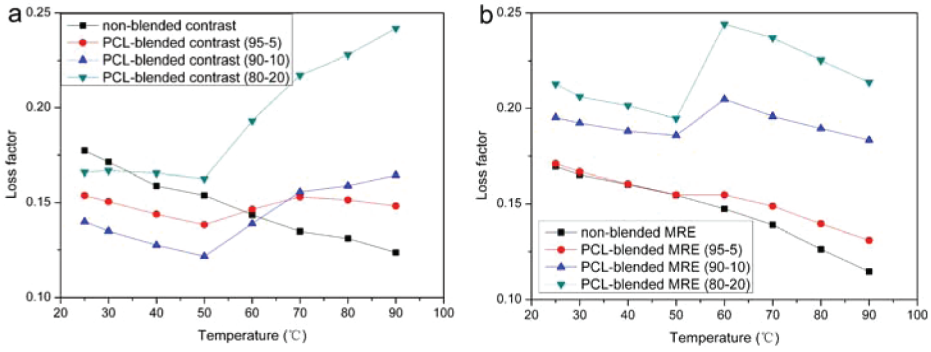

Figure 5. Loss factors of samples under different temperatures: (a) contrast samples; (b) MRE samples.

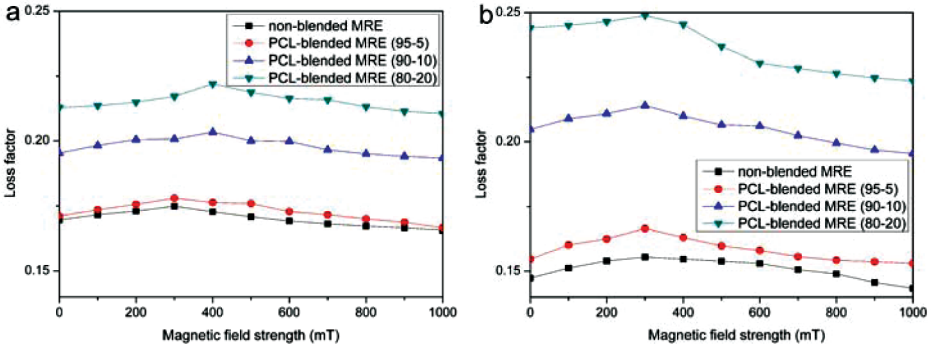

Figure 6. Loss factors of MRE samples under different magnetic field strengths: (a) testing at 25 °C; (b) testing at 60 °C.

at 60 °C. With increasing temperature, the energy dissipation increases. In the above analysis, the loss factor increases gradually when the temperature is above 60 °C for the PCL-blended contrast (Figure 5a). For the PCL-blended MRE, the loss factor suddenly increases at 60 °C and then decreases gradually with increasing temperature (Figure 5b). The particles in the PCL matrix can obstruct the movement of PCL molecular chains, and the energy dissipation is reduced. Compared with PCL-blended contrast, the obstruction of the particles is the main reason attributed to the decrease of the loss factor when the temperature is above 60 °C. Consequently, the damping properties are changed remarkably by the added PCL under different temperatures.

Additionally, the effect of PCL content on the loss factor under different temperatures was also investigated. When the temperature is below 60 °C, the loss factor decreases and then increases with increasing PCL for the contrast samples (Figure 5a), while the loss factor increases with increasing PCL for the MRE samples (Figure 5b). The movement of the PCL molecular chains is smaller than that of the BR molecular chains under the shear stress when PCL is in the semicrystalline solid state. Therefore, for the contrast samples, the loss factor decreases with increasing PCL when the PCL content is low. However, due to the poor compatibility, the interfacial sliding between PCL and BR increases with increasing PCL and this leads to increasing of the loss factor (Figure 5a). For the MRE samples, the interfacial sliding between PCL and the particles is enhanced when PCL is in the semicrystalline solid state. In this case, the interfacial friction plays a key role in increasing the loss factor (Figure 5b). Moreover, when the temperature rises to 60 °C, PCL is in a liquated soft material state and the friction between PCL molecular chains increases. Therefore, the loss factor of the samples increases with increasing PCL when the temperature is above 60 °C.

The magnetic field strength dependency of the loss factor is shown in Figure 6. The tests were conducted at a frequency of 10 Hz and constant shear strain amplitude of 0.5%. It can be seen that the loss factors of the MRE samples show a tendency of increase plus decrease with increasing magnetic field. This phenomenon has been reported in our previous work.[24,36] The change of loss factor is slight under different magnetic fields at room temperature (Figure 6a). When the temperature rises to 60 °C, it is noted that the change of loss factor of the PCL-blended MRE is larger than that of the nonblended MRE under different magnetic field strengths, which increases with increasing PCL (Figure 6b). The absolute change of loss factor under different magnetic fields is defined as $\Delta\text{Loss} = \text{Loss}_{max} - \text{Loss}_{min}$, in which Loss_{max} and Loss_{min} are the maximum value and minimum value of the loss factor under different magnetic fields, respectively. In Figure 6b, ΔLoss of the nonblended MRE and the PCL-blended MRE (80−20) are respectively 0.012 and 0.025. ΔLoss of the PCL-blended MRE (80−20) increases 108% in comparison with that of the nonblended MRE. In practical application, Sun et al.[37] observed that the vibration reduction effect of vibration absorbers increased obviously when the damping ratio reduced 0.005. As a result, the damping properties of the MREs can be controlled by tuning the magnetic fields and the controllability of the damping properties of the PCL-blended MRE is enhanced obviously.

3.2.2. Mechanism. The mechanism of the temperature-dependent and magnetic-field-dependent mechanical properties was discussed. A sketch of the microscopic particle chain structures of the MRE samples was obtained (Figure 7). Parts a and b of Figure 7 show the microscopic structures of the nonblended MRE, corresponding to before and after the preforming configuration, respectively. The particle chain structures of the nonblended MRE are locked into the matrix,

dx.doi.org/10.1021/ie300317b | Ind. Eng. Chem. Res. 2012, 51, 6395−6403

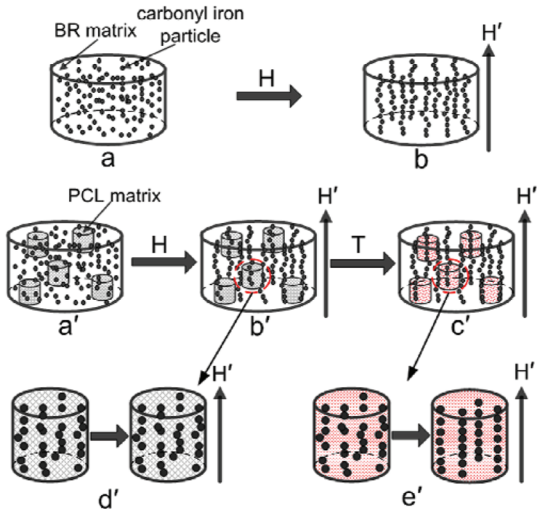

Figure 7. Sketch of the microscopic particle chain structures of the MRE samples: (a, b) microscopic structures of nonblended MRE, corresponding to before and after the preforming configuration, respectively; (a′–e′) microscopic structures of PCL-blended MRE, where (a′) is before the preforming configuration, (b′) and (c′) are after the preforming configuration, respectively, corresponding to the two states when the temperature is below and above PCL melting point, and (d′) and (e′) are the enlarged views of the distribution of particles in the PCL matrix, respectively corresponding to (b′) and (c′). *H* and *H*′ correspond to the preforming and testing magnetic fields, respectively.

which cannot be changed under the testing magnetic field (Figure 7b). Figure 7a′–e′ shows the microscopic structures of the PCL-blended MRE, where part a′ is before the preforming configuration and parts b′ and c′ are after the preforming configuration, corresponding to the two states when the temperature is below and above the PCL melting point, respectively. Parts d′ and e′ of Figure 7 are the enlarged views of the distribution of particles in the PCL matrix, which correspond to parts b′ and c′. For the PCL-blended MRE, the particle chain structures in the matrix cannot be changed under the testing magnetic field when the temperature is below the PCL melting point (Figure 7b′,d′). While the temperature is above the PCL melting point (Figure 7c′,e′), the particles in the PCL matrix can move easier and form perfect chain structures under the testing magnetic field, because PCL is in a liquated soft material.

The chain structures of the nonblended MRE are tightly locked within the matrix, and they cannot be changed under the testing magnetic field. For the PCL-blended MRE, the particle chain structures also cannot be moved under the testing magnetic field when the temperature is below the PCL melting point. Therefore, the change of loss factor of the MRE samples is slight under different magnetic field strengths at room temperature (Figure 6a). When the temperature is above the melting point, PCL transforms from the solid state to the liquated soft state. The particles can change their locations very easily. If the testing magnetic field is applied, the particles rearrange their positions and form more perfect chain structures. In that case, the interaction between the particles increases and the effect of particle obstruction is enhanced when the magnetic field strength is increased. Thus, the friction between the matrix molecular chains is reduced. The loss factor of the PCL-blended MRE reduces more than that of the nonblended MRE when the magnetic field strength is above 300 mT (Figure 6b). Therefore, the controllability of the damping properties of MREs is enhanced by added PCL.

3.2.3. Effect of Shear Strain Amplitude and Frequency on the Loss Factor. Under different temperatures and different magnetic field strengths (0 and 500 mT), the effects of shear strain amplitude and frequency on the loss factor were investigated (Figures 8 and 9). Figure 8 illustrates the shear

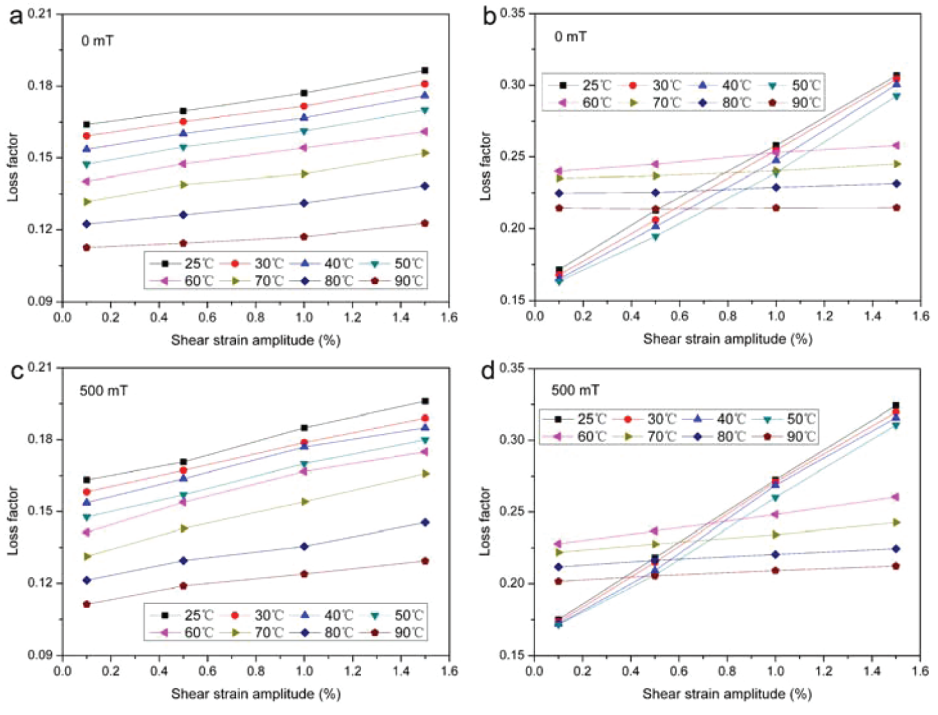

Figure 8. Loss factor of MRE samples under different shear strain amplitudes: (a, c) nonblended MRE; (b, d) PCL-blended MRE (80–20).

dx.doi.org/10.1021/ie300317b | *Ind. Eng. Chem. Res.* 2012, 51, 6395–6403

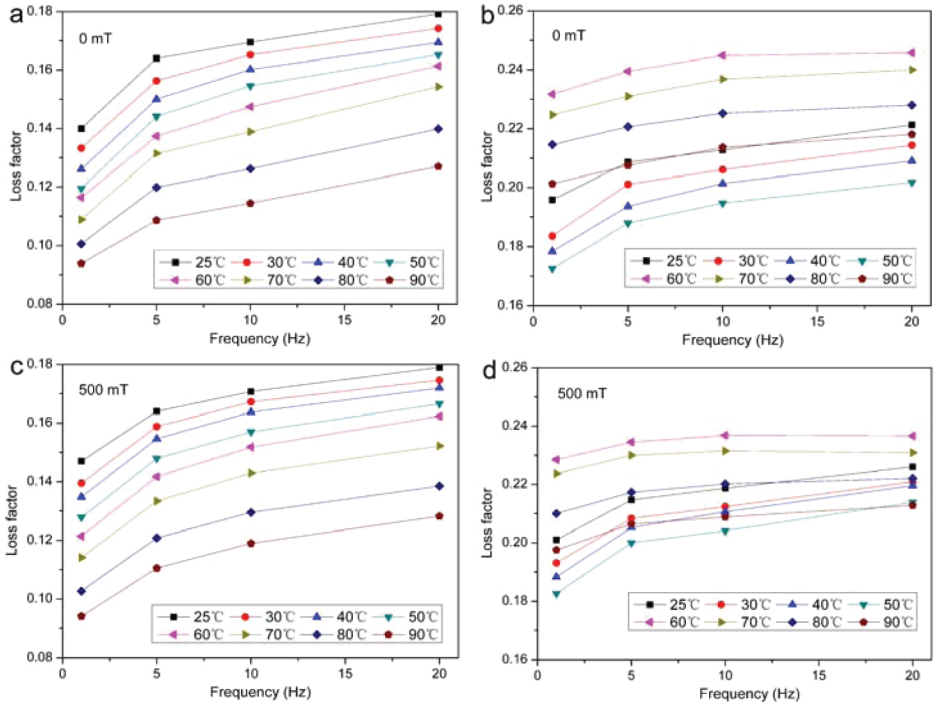

Figure 9. Loss factor of MRE samples under different frequencies: (a, c) nonblended MRE; (b, d) PCL-blended MRE (80−20).

strain amplitude dependency of the loss factor under different temperatures. The loss factor increases with increasing shear strain amplitude. It is noted that the strain-induced increases of nonblended MRE and PCL-blended MRE (80−20) in loss factor under different temperatures are different. For the nonblended MRE, the tendency of strain-induced increases in loss factor decreases slightly with increasing temperature (Figure 8a,c). However, the tendencies are definitely different for the PCL-blended MRE (80−20), when the temperatures are below and above the PCL melting point. The loss factor of the samples increases with increasing shear strain amplitude when the temperature is below the PCL melting point. As soon as the temperature is above the PCL melting point, the loss factor increases indistinctly with increasing shear strain amplitude. The compatibility between BR and PCL as well as between PCL and the particles is poor when the temperature is below the PCL melting point (Figure 2c−f). Thus the interfacial friction increases obviously when more interfacial areas are presented with increasing shear strain amplitude. If the temperature is above the PCL melting point, the deformation of the PCL matrix (liquated soft state) can catch up with the deformation of the BR matrix under the shear stress; thus the interfacial friction between BR and PCL can be ignored. In addition, the interfacial friction between PCL and the particles is constant almost under different shear strain amplitudes. Thus, the increases of the loss factor are indistinct with increasing shear strain amplitude when the temperature is above the PCL melting point. Comparing with Figure 8a,c and Figure 8b,d, it is noted that the tendencies of shear strain amplitude dependence of the loss factor are similar under different magnetic field strengths.

The frequency dependence of the loss factor is shown in Figure 9. An increased tendency of loss factor with increasing frequency can be seen. When the temperature is above the PCL melting point, the loss factor of PCL-blended MRE (80−20) increases slowly with increasing frequency, which is different from the nonblended MRE. Because PCL is in the molten state when the temperature is above the PCL melting point, there is more energy dissipation for the viscosity at low frequency. Under different magnetic field strengths (0 and 500 mT), the tendencies of loss factor with increasing frequency are similar.

Additionally, under different shear strain amplitudes and frequencies, the relative effect of loss factor was studied (Table 1). The relative effect of loss factor is defined as Re_{Loss} (%) = ($Loss_{500}$ − $Loss_0$)/$Loss_0$, where $Loss_0$ and $Loss_{500}$ are the loss factors under 0 and 500 mT magnetic field strengths, respectively. It can be observed that the Re_{Loss} (%) increases

Table 1. Relative Effects of Loss Factor of Samples under Different Shear Strain Amplitudes and under Different Frequencies

(a) Under Different Shear Strain Amplitudes

	Re_{Loss} (%)			
	nonblended MRE		PCL-blended MRE (80−20)	
shear strain amplitude (%)	25 °C	60 °C	25 °C	60 °C
0.1	−0.49	2.10	0.71	−5.04
0.5	0.71	2.44	4.41	−3.27
1.0	4.46	5.58	8.11	−1.90
1.5	5.03	5.64	8.70	0.97

(b) Under Different Frequencies

	Re_{Loss} (%)			
	nonblended MRE		PCL-blended MRE (80−20)	
freq (Hz)	25 °C	60 °C	25 °C	60 °C
1	5	4.3	2.66	−1.38
5	1.22	3.13	2.92	−2.09
10	0.71	2.99	2.77	−3.27
20	−0.11	0.56	2.12	−3.7

dx.doi.org/10.1021/ie300317b | Ind. Eng. Chem. Res. 2012, 51, 6395−6403

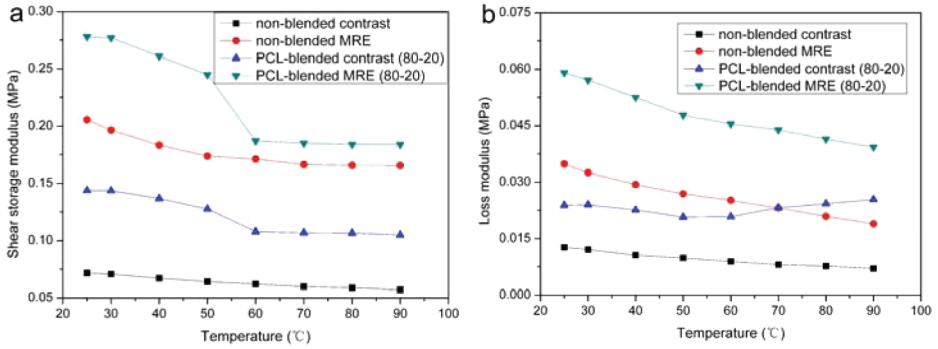

Figure 10. Performances of contrast samples and MRE samples under different temperatures: (a) shear storage modulus; (b) loss modulus.

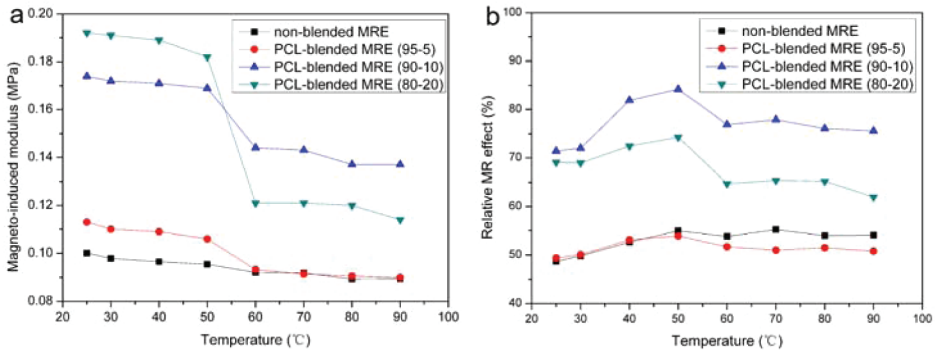

Figure 11. Magneto-induced modulus and relative MR effects of MRE samples under different temperatures.

with increasing shear strain amplitude (Table 1a), while it decreases with increasing frequency (Table 1b). The magnetic interaction force between the particles is enhanced when a magnetic field (500 mT) is applied. This interaction can increase slipping friction under the shear stress and obstruct the movement of rubber molecule chains. The slipping friction between the matrix and the particles increases with increasing shear strain amplitude. Thus, the slipping friction energy dissipation plays a key role in the strain-induced increase in Re_{Loss} (%). However, the tangled molecule chains of the matrix increase with increasing frequency. This results in the increase of the obstruction effect of the particles. Therefore, the obstruction of particles plays an important role in the frequency-induced decrease in Re_{Loss} (%). It is also noted that the Re_{Loss} (%) of the samples under different shear strain amplitudes and frequencies is very small.

3.3. Storage Modulus and Loss Modulus. The effect of temperature on the modulus properties of the samples was studied, as shown in Figure 10. The tests were conducted at a frequency of 10 Hz, constant shear strain amplitude of 0.5%, and constant magnetic field strength of 0 mT. Figure 10a shows the storage modulus of the samples under different temperatures. It can be seen that the storage modulus decreases with increasing temperature, which is a common characteristic of polymers. The storage modulus of the PCL-blended contrast (80−20) and PCL-blended MRE (80−20) decreases sharply at 60 °C because PCL is in the molten state. Comparing with the contrast samples and the MRE samples, the temperature-induced decrease in storage modulus of the MRE samples is larger. It is related to the reduced effect of particle reinforcement. Figure 10b shows the loss modulus of the samples under different temperatures. The loss modulus of the nonblended contrast and nonblended MRE decreases with increasing temperature. The higher the temperature is, the shorter the relaxation time of polymer molecule chains is. The content of the tangled BR molecular chains reduces with increasing temperature, and the BR molecular chains friction is reduced. Therefore, the loss modulus decreases with increasing temperature. For the PCL-blended contrast (80−20), the loss modulus increases gradually when the temperature is above the PCL melting point. This is because the friction between the PCL molecular chains increases. The particles in the PCL-blended MRE (80−20) can obstruct the movement of matrix molecular chains, which plays an important role in reducing the loss modulus. Thus the loss modulus of the PCL-blended MRE (80−20) decreases when the temperature is above the PCL melting point.

3.4. Magneto-Induced Modulus and MR Effect. The magneto-induced modulus and the relative MR effect of the MRE samples under different temperatures was also investigated (Figure 11). The tests were conducted at a frequency of 10 Hz and constant shear strain amplitude of 0.5%. The magnetic field was swept from 0 to 1000 mT. As shown in Figure 11a, the magneto-induced modulus decreases with increasing temperature. The magneto-induced modulus is defined as $\Delta G_m = G'_{max} - G'_0$, in which G'_0 is the initial storage modulus and G'_{max} is the storage modulus when the particles are in magnetic saturation. For the initial storage modulus G'_0, different initial values were used for different temperatures. With increasing temperature, the saturation magnetization strength of the particles decreases[38] and the matrix softens gradually. The reduced saturation magnetization strength of the particles will reduce the magneto-induced modulus of the samples. In addition, the effect of the particle reinforcement decreases for the softening of the matrix; it can be seen obviously that the magneto-induced modulus of the

dx.doi.org/10.1021/ie300317b | Ind. Eng. Chem. Res. 2012, 51, 6395−6403

PCL-blended MRE decreases sharply at 60 °C. During the preforming process, PCL is in the molten state and the particles can form chain structures more easily in the PCL matrix than in the BR matrix. Also, the stiffness of the unmelted PCL is larger than that of BR, which can enhance the effect of the particle reinforcement. Therefore, the magneto-induced modulus of the MRE samples increases with increasing PCL when the temperature is below the PCL melting point. All the analysis shows that the matrix modulus plays an important role in the magneto-induced moduli of MREs. For the same sample, the lower the matrix modulus is, the lower the magneto-induced modulus is, when the temperature increases gradually. Under application of a magnetic field, the decrement of the particle reinforcement effect for the matrix with lower modulus is larger. However, for the samples with different matrixes, not only the matrix modulus but also the particle distribution and the characteristic of the matrix play key roles in the magneto-induced modulus.

Figure 11b shows the relative MR effect, which is defined as RMe (%) = $\Delta G_m/G'_0$ of the MRE samples under different temperatures. The relative MR effect of nonblended MRE shows an increased and gradually stabilized tendency. In comparison to the nonblended MRE, the relative MR effect of PCL-blended MRE decreases sharply at 60 °C. This is because the temperature-induced decrease of the initial storage modulus G'_0 is lower than that of magneto-induced modulus at 60 °C (Figures 10a and 11a). When the temperature is below 60 °C, the temperature-induced decrease of the initial storage modulus is larger than that of the magneto-induced modulus. Thus the relative MR effect shows an increased tendency. The initial storage modulus and the magneto-induced modulus all decrease slightly with increasing temperature when it is above 60 °C. Therefore, the relative MR effect shows a gradually stabilized tendency. As a result, the controllability of the modulus properties and the MR effect of MREs are also enhanced by added PCL.

4. CONCLUSION

Novel MRE materials with different BR/PCL mass ratio matrixes were prepared, and their microstructures and dynamic properties were studied. Under different temperatures, magnetic fields, shear strain amplitudes, and frequencies, the effects of the PCL matrix on the loss factor and other dynamic properties were experimentally investigated. PCL belongs to a class of temperature-controllable materials which can transform from semicrystalline solid to liquated soft material by increasing the temperature above the melting point. The analysis results indicated that the damping properties were highly dependent on the PCL ratio, the temperature, and the magnetic field. Both the strain amplitude and frequency showed large influences on the loss factors. As soon as the temperatures increased above the PCL melting point, the strain-induced and frequency-induced loss factors changed a little. When the temperatures were below the PCL melting point, great changes took place in the strain-induced and frequency-induced loss factors. The influence of magnetic field on the loss factor was enhanced when PCL was in a liquated soft state. Thus, the MRE damping properties can be controlled by adding PCL. Furthermore, the changes of magneto-induced modulus and MR effect of the MRE samples increased with increasing PCL under different temperatures. This work provides a facile method to control the damping properties of the MRE materials, which will lead to them being widely applied in practical applications.

AUTHOR INFORMATION

Corresponding Author

*E-mail: gongxl@ustc.edu.cn (X.G.); xuansh@ustc.edu.cn (S.X.).

Notes

The authors declare no competing financial interest.

ACKNOWLEDGMENTS

Financial support from the National Natural Science Foundation of China (Grants 11125210, 11072234, 11102202), the National Basic Research Program of China (973 Program, Grant 2012CB937500), and the Specialized Research Fund for the Doctoral Program of Higher Education of China (Project No. 20093402110010) is gratefully acknowledged.

REFERENCES

(1) Shiga, T.; Okada, A.; Kurauchi, T. Magnetoviscoelastic behavior of composite gels. *J. Appl. Polym. Sci.* **1995**, *58*, 787.
(2) Zhou, G. Y. Shear properties of a magnetorheological elastomer. *Smart Mater. Struct.* **2003**, *12*, 139.
(3) Farshad, M.; Le Roux, M. Compression properties of magnetostrictive polymer composite gels. *Polym. Test.* **2005**, *24*, 163.
(4) Zhang, W.; Gong, X. L.; Xuan, S. H.; Xu, Y. G. High-performance hybrid magnetorheological materials: preparation and mechanical properties. *Ind. Eng. Chem. Res.* **2010**, *49*, 12471.
(5) Li, W. H.; Zhou, Y.; Tian, T. F. Viscoelastic properties of MR elastomers under harmonic loading. *Rheol. Acta* **2010**, *49*, 733.
(6) Gong, X. L.; Zhang, X. Z.; Zhang, P. Q. Fabrication and characterization of isotropic magnetorheological elastomers. *Polym. Test.* **2005**, *24*, 669.
(7) Jolly, M. R.; Carlson, J. D.; Muñoz, B. C. A model of the behaviour of magnetorheological materials. *Smart Mater. Struct.* **1996**, *5*, 607.
(8) Carlson, J. D.; Jolly, M. R. MR fluid, foam and elastomer devices. *Mechatronics* **2000**, *10*, 555.
(9) Zhang, W.; Gong, X. L.; Xuan, S. H.; Jiang, W. Q. Temperature-dependent mechanical properties and model of magnetorheological elastomers. *Ind. Eng. Chem. Res.* **2011**, *50*, 6704.
(10) Ginder, J. M.; Nichols, M. E.; Elie, L. D.; Tardiff, J. L. Magnetorheological elastomers: properties and applications. *Proc. SPIE* **1999**, *3675*, 131.
(11) Fang, F. F.; Choi, H. J.; Seo, Y. Sequential Coating of Magnetic Carbonyliron Particles with Polystyrene and Multiwalled Carbon Nanotubes and Its Effect on Their Magnetorheology. *ACS Appl. Mater. Interfaces* **2010**, *2*, 54.
(12) Lokander, M.; Stenberg, B. Performance of Isotropic Magneto-rheological Rubber Materials. *Polym. Test.* **2003**, *22*, 245.
(13) Lokander, M.; Stenberg, B. Improving the Magnetorheological Effect in Isotropic Magnetorheological Rubber Materials. *Polym. Test.* **2003**, *22*, 677.
(14) Lokander, M.; Reitberger, T.; Stenberg, B. Oxidation of Natural Rubber based Magnetorheological Elastomers. *Polym. Degrad. Stab.* **2004**, *86*, 467.
(15) Ginder, J. M.; Schlotter, W. F.; Nichols, M. E. Magneto-rheological elastomers in tunable vibration absorbers. *Proc. SPIE* **2001**, *4331*, 103.
(16) Ginder, J. M.; Clark, S. M.; Schlotter, W. F.; Nichols, M. E. Magnetostrictive phenomena in magnetorheological elastomers. *Int. J. Mod. Phys. B* **2002**, *16*, 2412.
(17) Albanese, A. M.; Cunefare, K. A. Properties of a magneto-rheological semiactive vibration absorber. *Proc. SPIE* **2003**, *5052*, 36.
(18) Deng, H. X.; Gong, X. L.; Wang, L. H. Development of an adaptive tuned vibration absorber with magnetorheological elastomer. *Smart Mater. Struct.* **2006**, *15*, N111.
(19) Lerner, A. A.; Cunefare, K. A. Performance of MRE-based vibration absorbers. *J. Intell. Mater. Syst. Struct.* **2008**, *19*, 551.

(20) York, D.; Wang, X. J.; Gordaninejad, F. A new MR fluid-elastomer vibration isolator. *J. Intell. Mater. Syst. Struct.* **2007**, *18*, 1221.
(21) Hu, W.; Wereley, N. M. Hybrid magnetorheological fluid-elastomeric lag dampers for helicopter stability augmentation. *Smart Mater. Struct.* **2008**, *17*, 045021.
(22) Blom, P.; Kari, L. Smart audio frequency energy flow control by magneto-sensitive rubber isolators. *Smart Mater. Struct.* **2008**, *17*, 015043.
(23) Kari, L.; Lokander, M.; Stenberg, B. Structure-Borne Sound Properties of Isotropic Magneto-Rheological Rubber. *Kautsch. Gummi Kunstst.* **2002**, *55*, 669.
(24) Fan, Y. C.; Gong, X. L.; Jiang, W. Q.; Zhang, W.; Wei, B.; Li, W. H. Effect of maleic anhydride on the damping property of magnetorheological elastomers. *Smart Mater. Struct.* **2010**, *19*, 055015.
(25) An, H. N.; Picken, S. J.; Mendes, E. Enhanced hardening of soft self-assembled copolymer gels under homogeneous magnetic fields. *Soft Matter* **2010**, *6*, 4497.
(26) Behl, M.; Ridder, U.; Feng, Y. K.; Kelch, S.; Lendlein, A. Shape-memory capability of binary multiblock copolymer blends with hard and switching domains provided by different components. *Soft Matter* **2009**, *5*, 676.
(27) Cao, F. N.; Jana, S. C. Nanoclay-tethered shape memory polyurethane nanocomposites. *Polymer* **2007**, *48*, 3790.
(28) Tong, X. M.; Zhang, X. W.; Ye, L.; Zhang, A. Y.; Feng, Z. G. Synthesis and characterization of block copolymers comprising a polyrotaxane middle block flanked by two brush-like PCL blocks. *Soft Matter* **2009**, *5*, 1848.
(29) Luo, X. F.; Lauber, K. E.; Mather, P. T. A thermally responsive, rigid, and reversible adhesive. *Polymer* **2010**, *51*, 1169.
(30) Luo, X. F.; Ou, R. Q.; Eberly, D. E.; Singhal, A.; Viratyaporn, W.; Mather, P. T. A thermoplastic/thermoset blend exhibiting thermal mending and reversible adhesion. *ACS Appl. Mater. Interfaces* **2009**, *1*, 612.
(31) Huang, M. H.; Li, S.; Hutmacher, D. W.; Coudane, J.; Vert, M. Degradation characteristics of poly(epsilon-caprolactone)-based co-polymers and blends. *J. Appl. Polym. Sci.* **2006**, *102*, 1681.
(32) Dai, W. F.; Huang, H.; Du, Z. Z.; Lang, M. D. Synthesis, characterization and degradability of the novel aliphatic polyester bearing pendant N-isopropylamide functional groups. *Polym. Degrad. Stab.* **2008**, *93*, 2089.
(33) Chen, L.; Gong, X. L.; Jiang, W. Q.; Yao, J. J.; Deng, H. X.; Li, W. H. Investigation on magnetorheological elastomers based on natural rubber. *J. Mater. Sci.* **2007**, *42*, 5483.
(34) Kim, J.; Shin, T. K.; Choi, H. J.; Jhon, M. S. Miscibility of biodegradable synthetic aliphatic polyester and poly(epichlorohydrin) blends. *Polymer* **1999**, *40*, 6873.
(35) Shin, T. K.; Kim, J.; Choi, H. J.; Jhon, M. S. Miscibility of biodegradable aliphatic polyester and poly(vinyl acetate) blends. *J. Appl. Polym. Sci.* **2000**, *77*, 1348.
(36) Fan, Y. C.; Gong, X. L.; Xuan, S. H.; Zhang, W.; Zheng, J.; Jiang, W. Q. Interfacial friction damping properties in magnetorheological elastomers. *Smart Mater. Struct.* **2011**, *20*, 035007.
(37) Sun, H. L.; Zhang, P. Q.; Gong, X. L.; Chen, H. B. A novel kind of active resonator absorber and the simulation on its control effort. *J. Sound Vib.* **2007**, *300*, 117.
(38) Liao, G. J.; Gong, X. L.; Xuan, S. H.; Guo, C. Y.; Zong, L. H. Magnetic-field-induced normal force of magnetorheological elastomer under compression status. *Ind. Eng. Chem. Res.* **2012**, *51*, 3322.